Organic Electronics 10 (2009) 73–84

Contents lists available at ScienceDirect

Organic Electronics

journal homepage: www.elsevier.com/locate/orgel

Thin-film transistors based on liquid-crystalline tetrafluorophenylter thiophene derivatives: thin-film structure and carrier transport

Fapei Zhang [a], Masahiro Funahashi [a,*], Nobuyuki Tamaoki [b,*]

[a] Department of Chemistry and Biotechnology, School of Engineering, University of Tokyo, 7-3-1 Hongo, Bunkyo-ku, Tokyo 113-8656, Japan
[b] Nanotechnology Research Institute, National Institute of Advanced Industrial Science and Technology, 1-1-1 Higashi, Tsukuba 305-8565, Ibaraki, Japan

ARTICLE INFO

Article history:
Received 25 July 2008
Received in revised form 6 October 2008
Accepted 7 October 2008
Available online 7 November 2008

PACS:
71.20.Rv
71.23.-k
72.20.Ee
72.80.Le
73.40.Sx
73.61.Ph

Keywords:
Liquid-crystalline semiconductors
Thin-film transistor
Carrier mobility
Smectic phase
Tetrafluorophenyl

ABSTRACT

The authors fabricated thin films by solution processes using liquid-crystalline (LC) semiconductors, 5-alkyl-5''-(4-hexyltetrafluorophenyl)-2,2':5',2''-terthiophene (**2–5**). Films of 5-propyl-5''-(4-hexyltetrafluorophenyl)-2,2':5',2''-terthiophene (**2**) show similar molecular packing as their non-fluorinated counterparts. However, the degree of molecular packing ordering from X-ray diffraction measurement is higher, and the films exhibit a more crystal-like structure. Moreover, fluorination has a remarkable effect on their mesomorphic behaviors. Films of **2** consist of large size LC domains (in the range of 100 μm) at room temperature. Thin-film transistors (TFTs) of **2** show p-type operation with good hole mobility up to 0.027 cm^2/Vs as well as improved operation stability under ambient conditions and high on/off ratio. Tetrafluorophenyl substitution leads to lowering of HOMO energy by 0.15 eV for **2** and 0.35 eV for **5**, resulting in operation stability. Variable-temperature current-voltage measurements indicate intrinsic carrier transport in films of **2**.

1. Introduction

In the quest for commercially successful organic field-effect transistors (OFETs), device fabrication by a solution process will be favorable due to its potential for large-area applicability and low cost production. However, the mobility of OFETs prepared by such a process is usually lower than that of devices fabricated by vacuum deposition. In addition, soluble conjugated polymers [1–3], solution-processable pentacene [4], and soluble precursors that can be converted into polycrystalline thin films [5] have been utilized to fabricate OFETs; however, a number of defects that inhibit smooth carrier transport are formed when polycrystalline thin films are formed.

Recently, liquid-crystalline (LC) semiconductors have emerged as promising materials for organic electronics [6–8]. They are solution-processable because of the thermal movement of the long alkyl chains attached to the LC molecules, which can self-assemble into large-area domains with a crystal-like structure and low defect density. Thus, the influence of grain boundaries, which seriously hinder charge carrier transport in polycrystalline materials,

* Corresponding authors. Tel.: +81 3 5841 7441; fax: +81 3 5841 8661.
E-mail addresses: funahashi@chembio.t.u-tokyo.ac.jp (M. Funahashi), n.tamaoki@aist.go.jp (N. Tamaoki).

1566-1199/$ - see front matter © 2008 Elsevier B.V. All rights reserved.
doi:10.1016/j.orgel.2008.10.020

is significantly suppressed [9]. Such capability of LCs to self-organize into ordered thin films is also favorable to electronic applications requiring homogeneity over large-area.

Bulk carrier mobility in columnar [10–12], smectic [13–16], nematic, and cholesteric [17–20] phases has been determined by the time-of-flight (TOF) technique. High carrier mobility, in excess of 0.1 cm^2/Vs, has been observed in highly ordered columnar and smectic phases of LC molecules with a large π-conjugated system. It should be noted that a domain structure with size exceeding several μm is often formed in LC phases, and the domain boundary does not inhibit electronic carrier transport [9] when compared with molecular crystals. Recently, large-area LC thin-film transistors (TFTs) were fabricated [21–23] by utilizing the self-organization properties of LC semiconductors, although most LC semiconductors recrystallize at room temperature, leading to an increase in the density of defects and carrier traps.

Recently, our group developed the LC material: 5-propyl-5''-(4-pentylphenyl)-2,2':5',2''-terthiophene (1) [23]. It exhibits a highly ordered smectic phase at room temperature and fast ambipolar transport with the hole and electron mobility of 0.07 cm^2/Vs and 0.2 cm^2/Vs in the bulk state, respectively. LC thin films with a thickness of 50 nm were fabricated by the spin-coating method and they can be applied to TFTs. The hole mobility of 0.04 cm^2/Vs was achieved on TFTs using this solution-processable LC semiconductor [24]. This good performance of the devices could be attributed to the highly ordered structure of the LC thin films with low defect density and domain size as compared to the channel length.

The stabilization of the LC thin films against oxidation is indispensable for the realization of practical FET devices working under ambient air for long time periods. For this, an increase in the oxidation potential by the introduction of electron withdrawing moieties is effective. The tetrafluorophenyl group has moderate electronegativity and does not deteriorate molecular linearity because of the small van der Waals radius of the fluorine atoms and its symmetry. In addition, it is known that when the terafluorophenyl moiety is introduced in LC molecules, it lowers their phase transition temperatures and increases their mobility [25]. It is expected that this property would result in the formation of large domains during LC thin-film formation. The effect of the tetrafluorophenyl group on the liquid crystallinity of phenylbithiophene derivatives [25] and conjugated polymers [26] has been studied. However, no examples of LC semiconductors with low molecular weight for TFTs exist.

In this work, we developed LC terthiophene derivatives with the tetrafluorophenyl group, 5''-(4-hexyltetrafluorophenyl)-2,2':5',2''-terthiophene derivatives (**2**–**4**), as well as a more electronegative LC terthiophene compound with both tetrafluorophenylene and perfluoroalkyl groups 5-perfluoro-hexyl-5''-(4-hexyl-tetrafluorophenyl)-2,2':5',2''-terthiophene (**5**), both of which are analogues of compound **1**. We performed a detailed investigation of the fluorination effect on LC phase transition, molecular packing, and film structure as well as their relationship with carrier transport in the TFTs.

2. Results and discussion

2.1. Material design and synthesis

As shown in Scheme 1, 5-(4-hexyl-2,3,5,6-tetrafluorophenyl)-5''-alkyl-2,2':5',2''-terthiophene (**2**–**4**) and 5-(4-hexyl-2,3,5,6-tetrafluorophenyl)-5''-perfluorohexyl-2,2':5',2''-terthiophene (**5**) were synthesized by a cross-coupling reaction between 5-bromo-5''-alkyl-2,2':5',2''-terthiophene and 1-hexyl-2,3,5,6-fluorobenzene catalyzed by palladium (II) acetate and di-*tert*-butylmethylphosphonium tetrafluoroborate in *N*,*N*-dimethylacetamide, a process reported by Fagnou et al. [27], because of the low reactivity of tetrafluorophenyl borate under a conventional Suzuki coupling reaction. In contrast, non-fluorinated compound **1** can be synthesized by the conventional Suzuki coupling reaction between alkylphenylboric acid and 5-bromo-5''-alkyl-2,2':5'2''-terthiophene [23]. Tetrafluorophenylterthiophene derivatives **2**–**5** were obtained in satisfactory yield and the crude products were purified by silica gel column chromatography and recrystallization from n-hexane.

2.2. Mesomorphic behaviors

The phase transition temperature was determined by differential scanning calorimetry (DSC) and the observation of optical textures under a polarized light microscope (POM). The LC phase structure was investigated by X-ray diffraction (XRD).

Compound **2** exhibits an enantiotropic nematic (N) phase and a highly ordered mesophase (M), as well as a

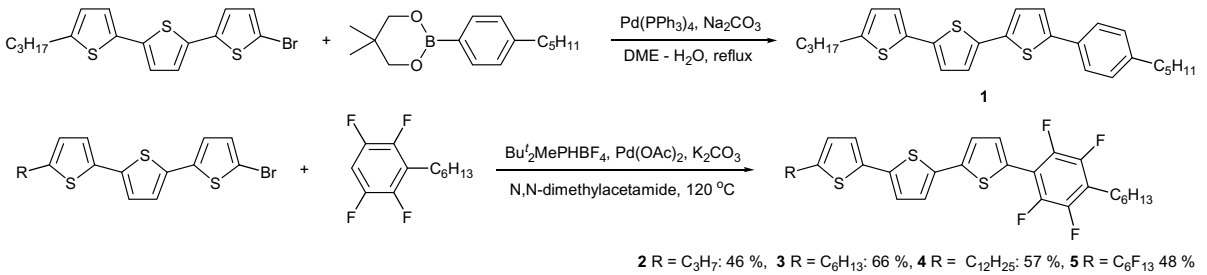

Scheme 1. Synthetic route of tetrafluorophenylterthiophene derivatives.

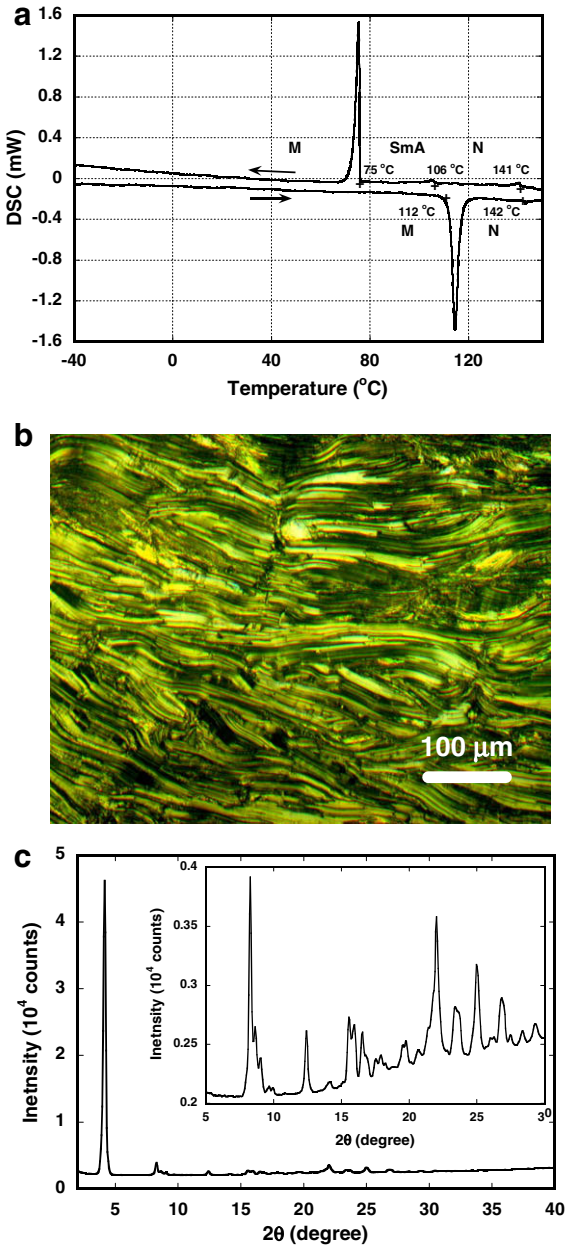

Fig. 1. (a) DSC profile of tetrafluorophenylterthiophene derivative **2**. (b) Micrographic textures in the mesophase of compound **2** at room temperature under a polarized light microscope. (c) X-ray diffraction in the mesophase of compound **2** at room temperature.

monotropic smectic A (SmA) phase. In the DSC curve of compound **2**, shown in Fig. 1(a), two peaks corresponding to an isotropic-N phase transition at 141 °C and a N-SmA at 106 °C with small transition enthalpies of 0.2 J/g as well as a peak corresponding to SmA-M transitions at 75 °C with a transition enthalpy of 8.4 J/g were observed in the cooling process. In the heating process, the curve exhibits one strong peak corresponding to the transition between the M phase and the N phases at 112 °C as well as a weak peak corresponding to the transition between the N and isotropic phases at 142 °C. When the M phase was cooled to −50 °C, no glass transition was observed. From the schlieren and fan-like textures under the observation of a polarized light microscope, the two phases that appear in the high-temperature region were identified as N and SmA phases, respectively. The result of X-ray diffraction also supports that these two phases are nematic and smectic phases, respectively. In the M phase, mosaic texture with defect lines as shown in Fig. 1b was observed. In the X-ray diffraction of the M phase of compound **2** (Fig. 1c), which appears below 75 °C in the cooling process, the strong diffraction (100) at $2\theta = 4.14°$ indicates a layer structure whose spacing is 23.1 Å. This value is slightly smaller than the molecular length (29.8 Å) with all-trans conformation, determined by MM2 calculation. And a number of peaks were observed between $2\theta = 10°$ and 30°, indicating that this phase has crystal-like 3-D structures. However, this phase exhibits fluidity above 100 °C on heating, below phase transition to the N phase, indicating that this is a mesophase with a freedom of molecular thermal movement. The optical micrographic texture revealed domains with a relatively large size exceeding several ten μm. Such a mesophase of 3-D order was observed in dithenylbenzene derivatives reported by Shimizu et al. [28]. It should be noted that this mesophase is retained below room temperature and compound **2** possessed no phase transition when it was cooled to −50 °C. The freedom of molecular thermal movement in the mesophase should cause the reorientation of molecules in the thin-film state in a thermal annealing process, resulting in large domain formation in the thin films.

Compound **3** also exhibits N, SmA, and highly ordered mesophase in both heating and cooling processes. Compound **4**, which has a long alkyl chain, exhibits a SmA and a highly ordered mesophase in a heating process. In a cooling process, an additional mesophase appears between the smectic A phase and the highly ordered mesophase. The phase transition temperatures are summarized in Table 1. The highly ordered mesophases of compounds **3** and **4** also exhibit fluidity to some extent below the phase transition

Table 1
Phase transition temperature of 5-(4-hexyltetrafluorophenyl)-5″-alkyl-2,2′:5′,2″-terthiophene derivatives.

	Heating	Cooling
2 R = C_3H_7	M 112 °C N 142 °C Iso	Iso 141 °C N 106 °C SmA 75 °C M
3 R = C_6H_{13}	M 114 °C SmA 130 °C N 139 °C Iso	Iso 138 °C N 130 °C SmA 90 °C M
4 R = $C_{12}H_{25}$	M_2 89 °C SmA 135 °C Iso	Iso 134 °C SmA 78 °C M_1 67°C M_2
5 R = C_6F_{13}	Cryst. 149 °C SmA 209 °C Iso	Iso 206 °C SmA 130 °C Cryst.

M, M_1, and M_2 are unidentified mesophases.

temperature between the highly ordered mesophase and the SmA phase. Therefore, the mesophases should also be a kind of plastic crystal phase with some extent of molecular thermal movement.

The phase transition temperatures were lowered by ca. 50 °C as compared with the non-fluorinated counterpart 5-(4-alkylphenyl)-5''-alkyl-2,2':5',2''-terthiophene [23]. For example, compound **2** exhibited a nematic phase between 112 °C and 142 °C and a highly ordered smectic phase below 112 °C, in contrast to 5-(4-propylphenyl)-5''-hexyl-2,2':5',2''-terthiophene (1), which exhibits a nematic phase between 217 °C and 202 °C and a highly ordered smectic phase below 202 °C [23]. Such a lowering of the phase transition temperature was reported in tetrafluorophenyl-bithiophene derivatives [25].

Compound **5**, which has a perfluoroalkyl chain, does not exhibit mesophases at room temperature. The phase at room temperature has a 3-D crystal-like order and no fluidity even near the phase transition to the SmA phase.

2.3. Structural characterization of mesomorphic thin films

The tetrafluorophenyl substituted compounds **2**-**4** show high solubility in common organic solvents. In this work, the investigation of the fabrication of the films and TFTs was focused on compound **2** due to the high similarity of molecular structure to non-fluorinated compound **1**. Homogeneous thin films of compounds **2** could be deposited on the surface of a SiO_2 layer treated with hexamethyldisalazane (HMDS) from their chlorobenzene solution by the spin-coating method. The polarized optical micrograph of as-prepared films of compound **2** in Fig. 2a shows the fine-threaded texture consisting of small domains with submicron size. Upon annealing at 85–90 °C for 10 min, a mosaic texture appears, corresponding to a highly ordered smectic phase (in Fig. 2b). This indicates that the thermal movement of the LC molecules caused the reorganization of macroscopic molecular alignment during the thermal annealing process below the phase transition temperature between the mesophase and the smectic A phase. This phenomenon should be associated with the freedom of molecular thermal movement in the mesophase. In particular, the films exhibited very large size of LC domains, exceeding several hundred μm, which was much larger than that in the film of non-fluorinated molecule **1** [23,24]. The tetrafluorophenyl group should increase molecular mobility in the mesophase because of weak intermolecular interaction.

The above facts were further confirmed by an atomic force microscope (AFM) observation. The film consists of large-area grains in the range of 20–50 μm (and even larger) with a lamellar structure. Fig. 2c and d show the AFM images within an individualized grain exhibiting a terrace structure on the surface. The height of the steps

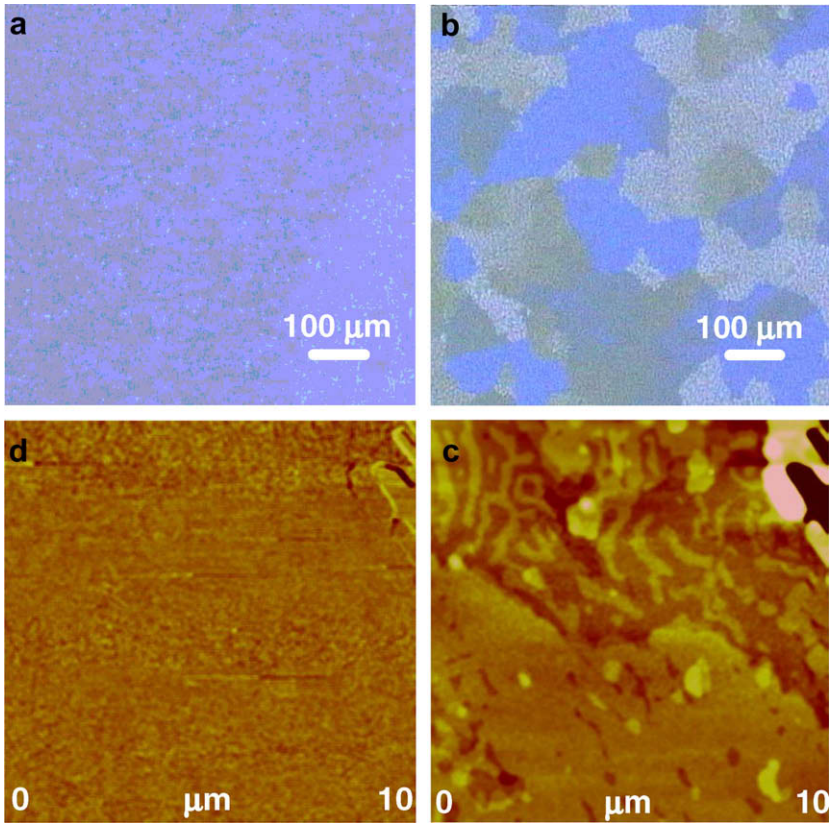

Fig. 2. Polarized-light microscopic textures at room temperature of thin film of compound **2** (a) as-cast and (b) annealed at 85 °C for 10 min. (c) AFM topographic and (d) phase images of thin film of compound **2**.

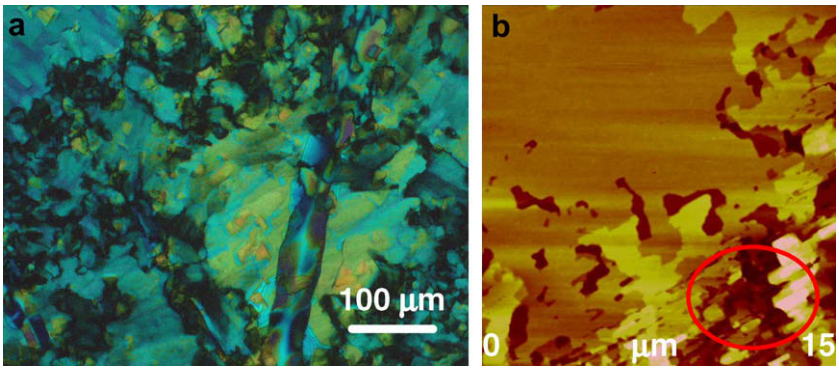

Fig. 3. (a) POM texture and (b) AFM topographic image of film of compound **5** from solution casting. The circled part is the less-ordered region.

separating the terraces is ca. 2.1 nm, corresponding to the thickness of one smectic layer of molecule **2** (vide infra). And the layers are thus parallel to the surface of the substrate. The large domain size is due to the higher mobility of the fluorinated molecules that originates from the weak interaction between tetrafluorophenyl groups. The high mobility of molecule **2** also causes partial dewetting of the film from the hydrophobic surface of the substrate during the annealing.

Homogenous thin films of compound **5** could not be fabricated by the spin-coating method at room temperature. Relatively homogenous films of the compound were prepared from the solution cast at 70 °C. They consist of domains with various sizes under POM observation, as shown in Fig. 3a. The AFM graph in Fig. 3b reveals the large size domains with a layer structure. The height of the steps is 2.5 nm, corresponding to the molecular length, larger than that in the film of compound **2**. However, we found some less-ordered regions (the circled part in Fig. 3b) between the highly ordered grains. In the less-ordered regions, the layers should be perpendicular to the surface, in contrast to the ordered regions, in which the layers are parallel to the surface of the substrate. In the FET devices, carriers move within the layers, and carrier movement should be inhibited in the less-ordered regions. This may be attributed to the stiffness of the rod-like fluoroalkyl chains in molecule **5**, which hinders effective molecular assembly during film growth Table 2.

Table 2
Molecular length, d-spacing, and molecular tilt angle in thin films of compounds **2**, **5**, and **1**.

Compound	Molecular length	d-Spacing	Tilt angle
2	2.8 nm	2.104 nm	38°
5	3.2 nm	2.660 nm	43°
1	2.7 nm	2.315 nm	31°

In the specular ($\theta/2\theta$) X-ray diffraction patterns (in Fig. 4a and b), the as-deposited films of compound **2** show two distinct series of intense peaks, suggesting the presence of two different LC phases. The dominant phase (denoted as Phase I) has an interlayer spacing (d-spacing) of 2.8 nm, larger than the second phase (phase II). Such a d-spacing value is nearly the same as that in the bulk mesophase (2.83 nm), in agreement with the POM observation. After the thermal annealing, phase I disappears completely and the intensity of the reflection peak from phase II is considerably enhanced, corresponding to complete phase transition into the mesophase. The annealed film shows a

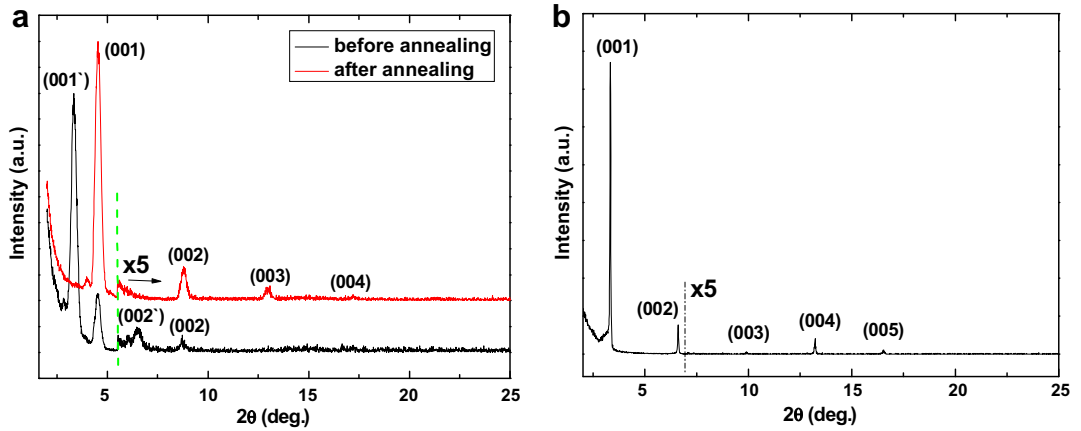

Fig. 4. X-ray diffraction of thin films of compounds **2** and **5**. (a) Out-of-plane pattern of film based on **2**, (b) out-of-plane pattern of film based on **5**.

strong reflection peak at an angle of $2\theta = 3.8°$ and three higher-order reflections attributed to (00n) reflections, indicating a clear layer structure. Using Bragg law, the interlayer spacing was calculated as 2.1 nm, in agreement with the step height of the molecular layers measured by AFM. This indicates that the molecular layer in the film is parallel to the substrate surface with the tilting of the molecular long axis with respect to the surface normal. In contrast, the XRD pattern exhibits only two (00n) reflection peaks for the film from fluorine-free molecule **1** [23,24]. These results indicate that the ordering of the stacking between the layers is enhanced by the fluorination of the phenyl group. The tilt angle of molecule **2** increases to 43° as compared to 31° in the case of molecule **1** (the molecular length of compound **1** is 2.7 nm), as shown in Table 1. The interdigitation of the alkyl chains of the LC molecules also lead to the shorter layer spacing. However, similar enhancement of the molecular tilt angle was found on films of fluoroarene-thiophenes [29].

For films of compound **5** with both tetraflurophenyl and fluoroalkyl substitutions, the XRD pattern (in Fig. 4(b)) shows more higher-order (00n) reflection peaks up to $n = 6$, suggesting a highly orientated film structure. The d-spacing is 2.7 nm, as calculated from the first-order reflection at an angle of 3.8°. Compared with the films of compound **2** (with only fluorophenyl ring), the tilt angle of molecule **5** is reduced to 38° (Fig. 5).

The in-plane structure of the films was studied using grazing incidence XRD (in Fig. 4). The annealed films of compound **2** show a reflection peak at an angle of about 16° (corresponding to a d-spacing of 0.56 nm). A few reflections appear in the range of the higher angle for the film of compound **5**, suggesting a long-range ordering within the molecular layers of films of compounds **2** and **5**. However, weak intensity of the diffraction peaks (due to the limitation of intensity of X-ray source) prevents detailed structural analysis. In addition, a strong peak appears at the low angle corresponding to a d-spacing of 1.9 nm. This indicates the possible existence of a minor phase with the molecular layer perpendicular to the substrate surface. Such a phase may be located at less-ordered regions between the highly ordered grains or at the dielectric-organic interface. Further investigation is required to elucidate its origin.

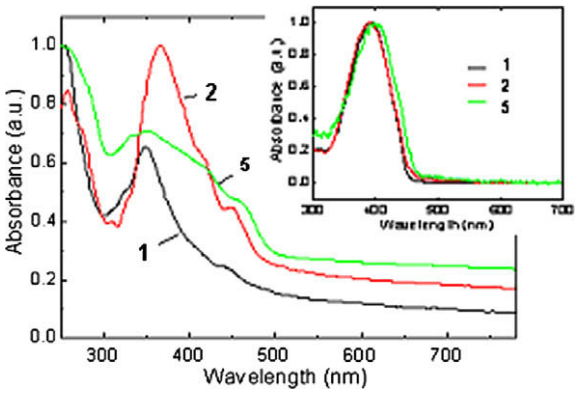

Fig. 6. Optical absorption spectra of compounds **1**, **2**, and **5** as films (inset shows optical absorption in chlorobenzene).

2.4. Absorption spectra of these compounds

Optical absorption spectra of compounds **1**, **2**, and **5** were measured both in solution and on thin films to study the effect of fluorophenyl and perfluoroalkyl-substitution on molecular packing and optical energy gap. The UV–VIS absorption spectra of the solutions (inset of Fig. 6) are free of fine structures. The absorption maximum (λ_{abs}) corresponds to the $\pi-\pi^*$ absorption band of the conjugated π-electron system of the core. The λ_{abs} of compound **2** in chlorobenzene is located at the same position as that of fluorine-free compound **1**.

UV–VIS data for the thin films of compounds **2** and **5** are shown in Fig. 6. The baselines of the spectra exhibit non-zero-values because of the light scattering. If the influence of the light scattering is excluded, the baselines should exhibit zero. All films show a similar absorption feature with a blue-shift of the maximum and a simultaneous red-shift of the onset compared to the solution spectra. The absorption maxima of films of compounds **2** and **5** are almost the

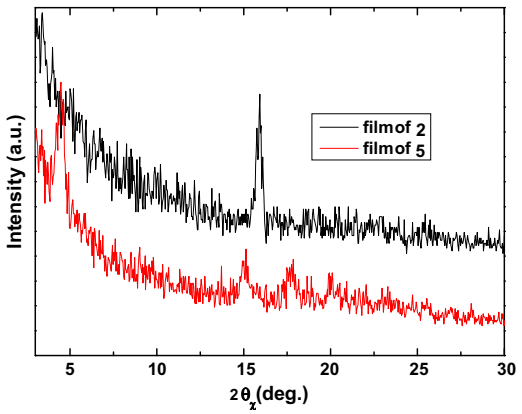

Fig. 5. In-plane X-ray diffraction patterns of films of compounds **2** and **5** (after annealing). The crystallographic assignments of the peaks are labeled.

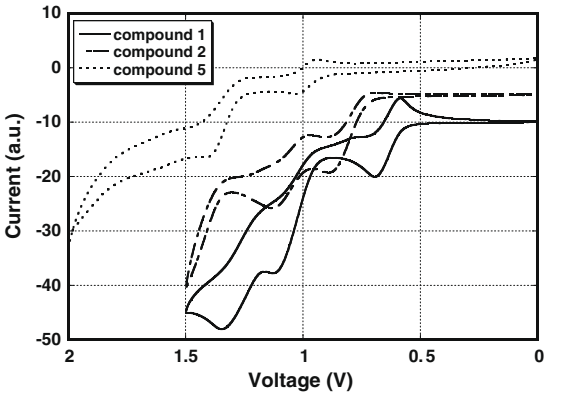

Fig. 7. Cyclic voltammogram of compounds **1**, **2**, and **5** in 0.05 M tetraethyl ammonium tetrafluoroborate/CH_2Cl_2 solution with an Ag/AgCl standard electrode. The scan rate was 0.01 V/min.

same and the optical band gap is estimated to be 2.6 eV for compounds **2** and **5**. This suggests a similar patterning of molecular packing in films of fluorinated molecules **2** and **5** as well as non-fluorinated material **1**.

A similar feature was observed for different kinds of oligothiophene films and it was attributed to the formation of H aggregates [22,30].

2.5. Measurement of oxidation potential

Fig. 7 shows cyclic voltammetry (CV) plots of compounds **1**, **2**, and **5**. Non-fluorinated molecule **1** and fluorinated molecules **2** and **5** exhibit quasi-reversible one-electron oxidation at 0.65 V, 0.80 V, and 0.99 V, respectively (vs. Ag/AgCl in 0.05 M $TEABF_4/CH_2Cl_2$ solution). This indicates the lowering of the HOMO energy by 0.15 eV and 0.35 eV upon substitution with the tetrafluorophenyl group and both the tetrafluorophenyl and perfluoroalkyl groups, respectively. Considering the similar optical gap for compounds **2** and **5**, as observed from the UV–VIS spectra, the LUMO level is also lowered by 0.15 eV and 0.35 eV for compounds **2** and **5** with respect to liquid crystal **1**, respectively. Considering the similar optical gap for compounds **1**, **2**, and **5**, as observed from the UV–VIS spectra, the LUMO level is also lowered by 0.15 eV and 0.35 eV for **2** and **5** with respect to **1**, respectively. This is consistent with the results of oligothiophene systems with a strong electron withdrawing tetrafluorophenyl or perfluoroalkyl group [31,32]. Such modification of the HOMO and LUMO levels will have a significant effect on the carrier transport process of organic semiconductors. The lowering of the HOMO levels of compound **2** should contribute to the stabilization of LC semiconductors for oxidation under air.

2.6. Time-of-flight measurement

The bulk carrier mobility in the mesophase of tetrafluorophenylterthiophene derivative **2** was measured by the conventional time-of-flight technique [33].

Under the application of an electric field, the photogenerated carriers drift across the bulk of the sample, inducing a transient photocurrent through the serial resistor. When the charge carriers reach the counter electrode, the induced photocurrent decays to zero. Therefore, a kink point in the transient photocurrent curve corresponds to the transit time t_T. Using Eq. (1), the carrier mobility (μ) can be calculated from the values of t_T, sample thickness d, and applied voltage V:

$$\mu = \frac{d^2}{Vt_T} \tag{1}$$

Illuminating the electrode under a positive or negative bias facilitates the determination of positive or negative carrier mobility, respectively.

When the absorption coefficient of a sample is sufficiently large, the excitation pulse is absorbed and a sheet of photo-carriers is generated at the interface between the illuminated electrode and the liquid crystal layer. In this study, a neat film of the compound exhibits a strong absorption band at around 370 and 250 nm in the smectic phase; the depth of penetration of the excitation light at 356 nm was estimated to be less than 0.5 μm, i.e., it was much smaller than the sample thickness (25 μm).

The highly ordered smectic phase of the compound has a relatively rigid structure with high viscosity; further, no change in the micrographic texture is observed when an electric field of the order of 10^5 V/cm is applied to the sample. The liquid crystal molecules in the sample are aligned parallel to the electrode surface; therefore, carrier transport within a smectic layer perpendicular to the electrode surface should be observed in the TOF measurement.

Fig. 8a shows transient photocurrents for the hole in the mesophase of compound **2** at room temperature. The obtained photocurrents are dispersive; however, transit times are estimated in a double logarithmic plot. The hole mobility is 0.07 cm^2/Vs, which is independent of the electric field and temperature between 100 and 50 °C. Below 50 °C, it decreases to 0.03 cm^2/Vs at room temperature. This decrease in the hole mobility should be attributed to the formation of defects that are caused by shrinkage when the sample was cooled, but not the intrinsic property of the liquid crystal material. If the defects are not formed with volume shrinkage, the hole mobility would be maintained constant.

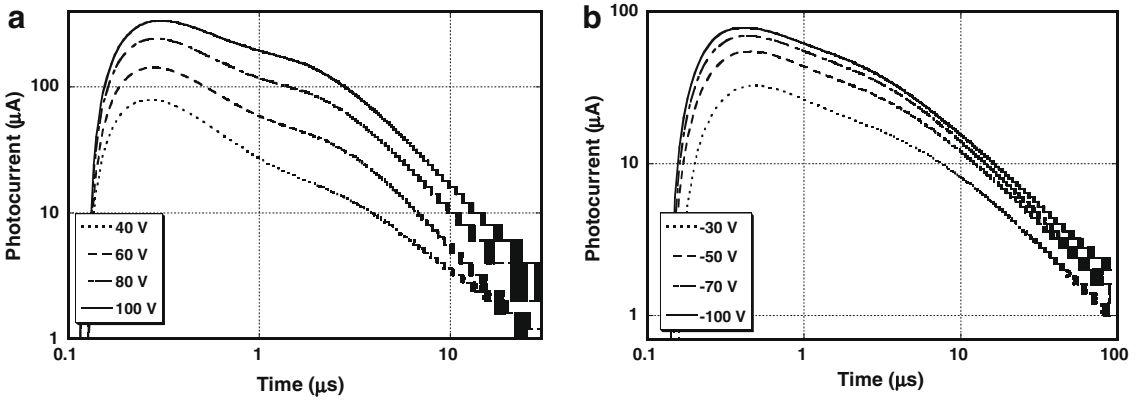

Fig. 8. Transient photocurrent curves in the mesophase of compound **2** at room temperature (a) for hole and (b) for electron. The sample thickness was 25 μm.

Fig. 8b shows transient photocurrents for the electron in the highly ordered mesophase around room temperature. The electron mobility at room temperature is 0.02 cm^2/Vs, which is independent of the electric field but not the temperature. The electron mobility is lower than that of the hole, suggesting that the electron transport process should be influenced from the electron traps in the bulk state.

In the crystal phase of compound **5**, only photocurrent decay is observed. Because of the crystallinity of compound **5**, the sample contains a number of defects that form deep traps, in contrast to the low defect density of the mesophase of compounds **1** and **2**.

2.7. FET characterization

The TFTs from compounds **2** and **5** were fabricated in the top-contact configuration. As shown in the section of the structural characterization of mesomorphic thin films, molecules are perpendicular to the substrates in the mesomorphic thin films. Therefore the carriers should move within the layers consisting of the liquid crystal molecules in the channel area. Fig. 9a shows the I_D–V_D characteristics for TFTs of compound **2** measured in ambient air. The devices exhibit a typical p-type operation. The hole mobility is calculated as 1.6–2.1 $\times 10^{-2}$ cm^2/Vs for most devices in a saturation region (see Fig. 9b). The current on/off ratio is more than 10^6. The highest value of the mobility is up to 2.7 $\times 10^{-2}$ cm^2/Vs in the best devices. Such a value is close to that obtained from the time-of-flight (TOF) measurement in the bulk state (0.07 cm^2/Vs at 50 °C), which represents the upper limit of transport properties of the TFTs [24]. This should be attributed to the formation of highly ordered LC domains with size larger than the channel length (20–30 μm) of the TFTs and thus, the effect of the grain boundary is significantly suppressed. The mobility is also comparable to that of the TFTs of non-fluorinated compound **1** [23,24]. Moreover, the TFTs of compound **2** exhibit enhanced stability of operation in ambient air. They can switch on continuously with less decay of drain current and mobility as compared to the TFTs of **1**. The devices using compound **2** can maintain characteristics such as mobility, on/off ratio, and threshold voltage for 1 month. The on/off ratio is also higher than those of devices using compound **1** (10^5–10^6) fabricated under the same condition (on HMDS-treated SiO_2). This may be due to the strong electron withdrawing characteristics of the tetrafluorophenyl group, which raises the oxidation potential of the aromatic core to make the material less susceptible to air oxidation.

The TFTs of compound **3** and **4** also exhibited p-type operation with the lower carrier mobilities. The mobilities were 1×10^{-2} cm^2/Vs for compound **3** and 8×10^{-3} cm^2/Vs for compound **4**, respectively.

On the other hand, TFTs of compound **5** show a much lower performance. The hole mobility is only about 1×10^{-5} cm^2/Vs and on/off ratio is 10^2. Presently, the exact origin of this low performance is not clear. One possible reason may be the existence of disordered regions and the smaller size of grains in the film, by which large amounts of electrical traps will be formed to hinder charge transport.

To evaluate the conduction mechanism and trap states in the films of compounds **2** and **5**, temperature-variable electrical characterization was performed for the TFTs from room temperature to 120 °C in a hot stage (in Fig. 10). The hole mobility of the TFTs of **2** remains nearly constant from room temperature to 70 °C and then decreases slightly (measurement was not performed at temperatures above 80 °C because of the dewetting of the film from the substrate). The threshold voltage also remains unchanged. Such behavior is in contrast to the thermally activated behavior observed on normal OTFTs of polycrystalline films [34–37], but similar to the characteristic carrier transport of LC semiconductors in the bulk, where field- and temperature-independent mobility are often observed [10–15]. This indicates that the electrical trap may not be a dominant factor to control carrier transport in such LC films, although some amount of trap states still exists at the dielectric-LC interface [38]. This should be due to the formation of highly ordered domains with a large size that exceeds the electrode gap. Such a behavior is attrib-

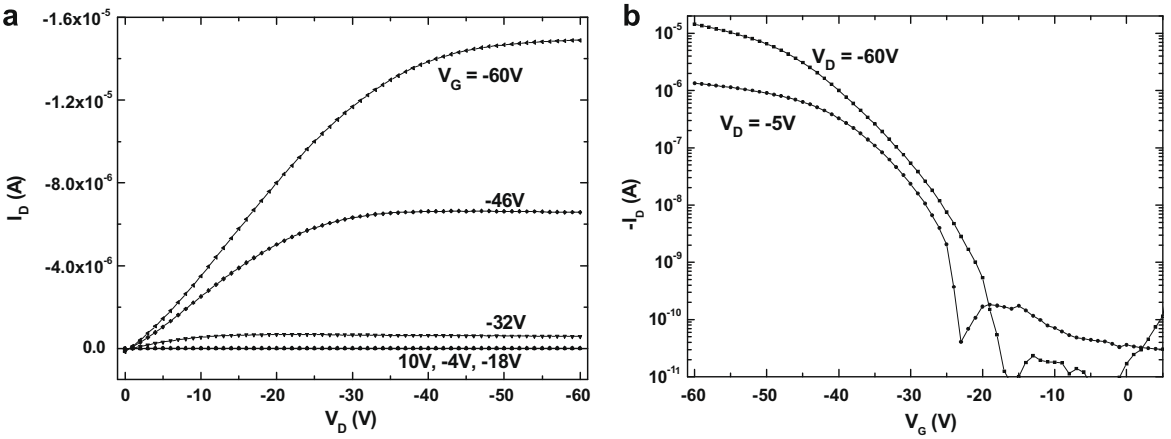

Fig. 9. (a) The output and (b) transfer characteristics of the TFT of compound **2** measured in ambient air. Channel length and width are 30 μm and 5 mm, respectively.

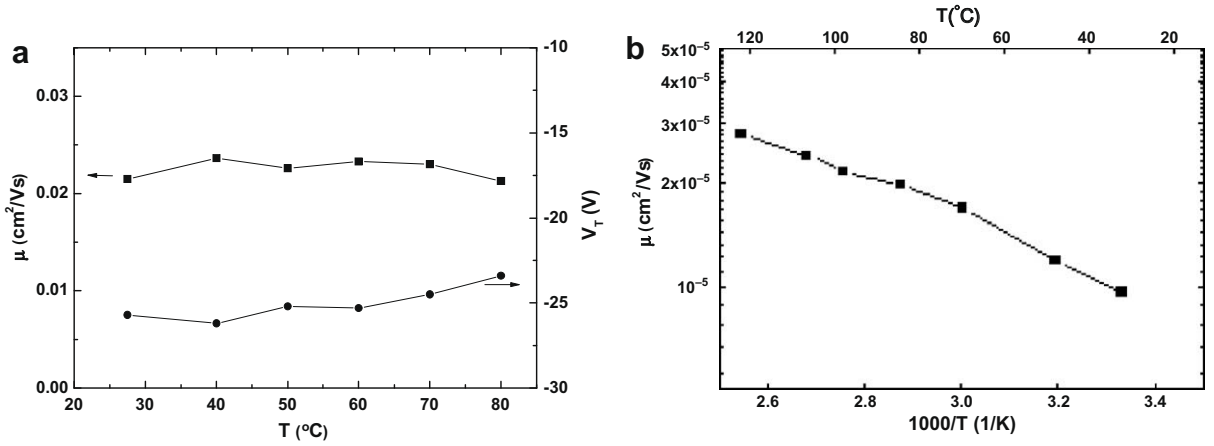

Fig. 10. Temperature dependence of saturation mobility and threshold voltage of TFTs based on (a) **2** and (b) **5**.

uted to self-healing of the positional disorder by thermal movement of the LC molecules. It should be emphasized that this introduction of the tetrafluorophenyl moiety should increase the mobility of the liquid crystal molecules, resulting in the formation of large domains greater than the channel length and a reduction in the defect density.

However, the mobility of the TFTs of compound **5** shows thermally activated behavior. It increases nearly exponentially with temperature ($\mu \propto \exp(E_A/kT)$) at an activation energy E_A of 50 meV. Therefore the carrier transport is trap-dominated, indicating the presence of large amounts of traps in the films. This is consistent with the microscopic observation shown above.

In this work, n-type operation was not observed in TFTs of compound **2** in ambient air and even in vacuum (10^{-3} Torr) although the gold, calcium, and samarium were used as the source and drain electrodes. This is different from the ambipolar behavior in their bulk state with an electron mobility of 0.02 cm^2/Vs, as obtained by the TOF technique. The result is also in contrast to cases of TFTs from dipentafluorophenyloligo thiophene or diperfluorohexyloligothiophene [29,39,40], in which a high electron mobility of 0.4 cm^2/Vs was obtained. It should be noted that our compound **2** showed a similar lowering of the LUMO energy relative to its non-fluorinated counterpart **1**, as observed in the cases of perfluoroarene substitution.

The absence of n-type behavior in the TFTs may be partially attributed to the high barrier of electron injection due to the relatively high-lying LUMO level of our materials. However, the dominant factor must lie in the attack by environmental oxygen because the solution processing of our TFTs was done in ambient air. For molecule **2**, an alkyltetrafluorophenyl group on one side of terthiophene is unable to provide sufficient screening of environmental O_2 or residual oxygen to the dielectric, which inhibits electron transport near the organic-dielectric interface [41]. Similarly, the absence of electron transport was observed in TFTs of oligthiophenes bearing a central tetrafluorophenylene ring [29,32]. For compound **5** with both tetrafluorophenyl and perfluoroalkyl substitutions, the absence of n-type behavior may be attributed to a large amount of structural defects during film growth; these defects act as electron traps. Improved processing conditions (e.g., inert atmosphere) and better control of growth parameters of thin films should be provided to reduce the defect density in the LC domains as well as oxygen attack, in order to achieve n-type operation in the TFTs.

3. Experimental section

3.1. Synthesis

All solvents were used as obtained. 5-Propyl-5''-bromo-2,2':5',2''-terthiophene; 5-hexyl-5''-bromo-2,2':5',2''-terthiophene; and 5-dodecyl-5''-bromo-2,2':5',2''-terthiophene were synthesized by the procedure reported by Y. Geng et al. [42]. Other chemicals were used as obtained without further purification. ^{1}H NMR spectra were measured on a Varian NMR-300 spectrometer using chloroform-d as a solvent. IR spectra were measured using a Shimadzu IR-600 spectrometer. Mass spectra were recorded on a Voyager MALDI TOF Mass equipment.

3.2. 5-Propyl-5''-(4-hexyl-2,3,5,6-tetrafluorophenyl)-2,2':5',2''-terthiophene (2)

A mixture of 5-bromo-5''-propyl-2,2':5',2''-terthiophene, 0.49 g (1.3 mmol); 1-hexyl-2,3,5,6-tetrafluorobenzene, 0.49 g (2.1 mmol); palladium acetate, 16.6 mg (0.074 mmol); di(*t*-butyl)methylphosphonium tetrafluoroborate, 40.3 mg (0.16 mmol); and potassium carbonate, 2.3 g (17 mmol), was dissolved in dimethyl acetamide, 10 ml, and stirred for 2 h at 130 °C. After cooling to room temperature, water was added to the reaction mixture. The precipitates were filtered off and the crude product was purified by column chromatography on silica gel with hot hexane. Recrystallization of the product from hexane afforded 0.25 g (0.59 mmol, 46%) of pure product as yellow crystals.

^{1}H NMR (300 MHz, $CDCl_3$) δ (ppm): 0.89 (3H, t, J = 6.8 Hz), 1.00 (3H, t, J = 7.4 Hz), 1.26–1.44 (6H, m),

1.56–1.66 (2H, m), 1.72 (2H, sext, J = 7.4 Hz), 2.74 (2H, t, J = 7.8 Hz), 2.78 (2H, t, J = 7.4 Hz), 6.69 (1H, d, J = 3.6 Hz), 7.00 (1H, d, J = 3.8 Hz), 7.01 (1H, d, J = 4.0 Hz), 7.12 (1H, d, J = 3.8 Hz), 7.18 (1H, d, J = 4.0 Hz), 7.50 (1H, d, J = 4.0 Hz). ^{13}C NMR (300 MHz), $CDCl_3$) δ (ppm): 13.7, 14.1, 22.6, 22.9, 24.9, 29.0, 29.3, 31.5, 32.3, 119.1, 119.3, 123.4, 123.7, 123.8, 125.0, 125.1, 130.6, 130.7, 130.8, 134.4, 134.6, 137.8, 139.5, 139.6, 145.7. IR (KBr disc) 2957.3, 2927.4, 2869.6, 2858.9, 1652.7, 1477.2, 1442.5, 1394.3, 1378.9, 1251.6, 1224.6, 1196.6, 1155.2, 1123.3, 1055.8, 1024.0, 944.9, 856.2, 787.8, 735.7, 725.1, 479.2 cm^{-1}. MS (MALDI): m/z (%): 522.6 (100%), 523.6 (29.5%), 524.6 (13.6%), 525.6 (4.9%) [M^+] ($C_{27}H_{26}F_4S_3$). Anal. Calcd. for 522.68: C 62.04, H 5.01, F 14.54, S 18.40; found: C 62.52, H 4.99.

3.3. 5-Hexyl-5''-(4-hexyl-2,3,5,6-tetrafluorophenyl)-2,2':5',2''-terthiophene (3)

A mixture of 5-bromo-5''-hexyl-2,2':5',2''-terthiophene, 0.51 g (1.2 mmol); 1-hexyl-2,3,5,6-tetrafluorobenzene, 0.51 g (2.15 mmol); palladium acetate, 18.1 mg (0.081 mmol); di(t-butyl)methylphosphonium tetrafluoroborate, 46.3 mg (0.18 mmol); and potassium carbonate, 0.55 g (4 mmol), was suspended in dimethyl acetamide, 5 ml, and stirred for 2 h at 130 °C. After cooling to room temperature, water was added to the reaction mixture. The precipitates were filtered off and the crude product was purified by column chromatography on silica gel with hot hexane. Recrystallization of the product from hexane afforded 0.45 g (0.80 mmol, 67%) of pure product as yellow crystals.

^{1}H NMR (300 MHz, $CDCl_3$) δ (ppm): 0.89 (3H, t, J = 6.8 Hz), 1.00 (3H, t, J = 7.4 Hz), 1.24–1.44 (12H, m), 1.56–1.66 (2H, m), 1.72 (2H, sext, J = 7.4 Hz), 2.75 (2H, t, J = 7.8 Hz), 2.80 (2H, t, J = 7.4 Hz), 6.69 (1H, d, J = 3.6 Hz), 7.00 (1H, d, J = 3.8 Hz), 7.02 (1H, d, J = 4.0 Hz), 7.13 (1H, d, J = 3.8 Hz), 7.19 (1H, d, J = 4.0 Hz), 7.50 (1H, d, J = 4.0 Hz). ^{13}C NMR (300 MHz), $CDCl_3$) δ (ppm): 13.6, 13.7, 22.1, 22.2, 22.4, 28.3, 28.4, 28.5, 28.8, 29.8, 31.0, 31.1, 118.6, 118.8, 122.9, 123.2, 123.3, 124.5, 124.6, 130.1, 130.2, 130.3, 133.8, 134.1, 137.3, 139.1, 139.5, 145.5. IR (KBr disc) 2957.3, 2926.5, 2891.5, 2855.1, 1652.7, 1476.2, 1444.4, 1389.5, 1377.9, 1225.5, 946.9, 858.2, 787.8, 758.9, 505.3, 490.8, 476.3 cm^{-1}. MS (MALDI): m/z (%): 564.6 (100%), 565.6 (29.5%), 566.6 (13.6%), 567.6 (4.9%) [M^+] ($C_{30}H_{32}F_4S_3$). Anal. Calcd. for 564.76: C 63.80, H 5.71, F 13.46, S 17.03; found: C 64.30, H 5.70.

3.4. 5-Dodecyl-5''-(4-hexyl-2,3,5,6-tetrafluorophenyl)-2,2':5',2''-terthiophene (4)

A mixture of 5-bromo-5''-dodecyl-2,2':5',2''-terthiophene, 0.52 g (1.05 mmol); 1-hexyl-2,3,5,6-tetrafluorobenzene, 0.46 g (1.9 mmol); palladium acetate, 18.1 mg (0.081 mmol); di(t-butyl)methylphosphonium tetrafluoroborate, 49.5 mg (0.20 mmol); and potassium carbonate, 0.4 g (4 mmol), was dissolved in dimethyl acetamide, 5 ml, and stirred for 2 h at 130 °C. After cooling to room temperature, water was added to the reaction mixture. The precipitates were filtered off and the crude product was purified by column chromatography on silicagel with hot hexane. Recrystallization of the product from hexane afforded 0.45 g (0.69 mmol, 66%) of pure product as yellow crystals.

^{1}H NMR (300 MHz, $CDCl_3$) δ (ppm): 0.89 (3H, t, J = 6.8 Hz), 1.00 (3H, t, J = 7.4 Hz), 1.22–1.44 (24H, m), 1.56–1.66 (2 H, m), 1.72 (2H, sext, J = 7.4 Hz), 2.75 (2H, t, J = 7.8 Hz), 2.79 (2H, t, J = 7.4 Hz), 6.69 (1H, d, J = 3.6 Hz), 7.00 (1H, d, J = 3.8 Hz), 7.02 (1H, d, J = 4.0 Hz), 7.13 (1H, d, J = 3.8 Hz), 7.19 (1H, d, J = 4.0 Hz), 7.50 (1H, d, J = 4.0 Hz). ^{13}C NMR (300 MHz), $CDCl_3$) δ (ppm): 13.6, 13.7, 22.1, 22.3, 22.4, 28.5, 28.7, 28.8, 28.9, 29.1, 29.2, 29.3, 29.4, 29.8, 31.0, 31.2, 31.5, 118.5, 118.8, 122.9, 123.2, 123.3, 124.4, 124.5, 130.1, 130.2, 130.3, 133.8, 134.1, 137.3, 139.1, 145.5. IR (KBr disc) 2956.4, 29871.5, 2848.4, 1480.1, 1468.5, 1446.4, 1227.5, 1130.1, 993.2, 944.0, 856.2, 810.0, 801.3, 791.6, 727.6, 478.3 cm^{-1}. MS (MALDI): m/z (%): 648.7 (100%), 649.7 (29.5%), 650.6 (13.6%), 651.7 (4.9%) [M^+] ($C_{36}H_{44}F_4S_3$). Anal. Calcd. for 648.92: C 66.63, H 6.83, F 11.71, S 14.82; found: C 67.04, H 6.94.

3.5. 5-Perfluorohexyl-5''-(4-hexyl-2,3,5,6-tetrafluorophenyl)-2,2':5',2''-terthiophene (4)

A mixture of 5-bromo-5''-perfluorohexyl-2,2':5',2''-terthiophene, 0.52 g (1.05 mmol); 1-hexyl-2,3,5,6-tetrafluorobenzene, 0.46 g (1.9 mmol); palladium acetate, 18.1 mg (0.081 mmol); di(t-butyl)methylphosphonium tetrafluoroborate, 49.5 mg (0.20 mmol); and potassium carbonate, 0.4 g (4 mmol), was dissolved in dimethyl acetamide, 5 ml, and stirred for 2 h at 130 °C. After cooling to room temperature, water was added to the reaction mixture. The precipitates were filtered off and the crude product was purified by column chromatography on silicagel with hot hexane. Recrystallization of the product from hexane afforded 0.45 g (0.69 mmol, 66%) of pure product as yellow crystals.

^{1}H NMR (300 MHz, $CDCl_3$) δ (ppm): 0.96 (3H, t, J = 6.9 Hz), 1.24–1.45 (6H, m), 1.69 (2H, sext, J = 6.3 Hz), 2.82 (2H, t, J = 7.5 Hz), 7.25–7.33 (4H, d, m), 7.52 (1H, d, J = 4.0 Hz), 7.69 (1H, d, J = 4.0 Hz). ^{13}C NMR (300 MHz), $CDCl_3$) δ (ppm): 13.7, 14.1, 22.6, 22.9, 24.9, 29.0, 29.3, 31.5, 32.3, 119.1, 119.3, 123.4, 123.7, 123.8, 125.0, 125.1, 130.6, 130.7, 130.8, 134.4, 134.6, 137.8, 139.5, 139.6, 145.7. IR (KBr disc) 2960.2, 2939.9, 2930.3, 2910.1, 2856.1, 1476.3, 1456.0, 1361.5, 1234.2, 1210.1, 1179.3, 1138.8, 787.8 cm^{-1}. MS (MALDI): m/z (%): 766.4 [M-S$^+$] ($C_{30}H_{19}F_{17}S_2$).

3.6. Characterization of mesomorphic behaviors

Phase transition behaviors of the liquid crystals were observed in micrographic optical textures under a polarized light microscope (Nikon OPTIPHOT2-POL) with a hot stage (Mettler F82HT hot stage) and thermograms were recorded by DSC (Seiko Instrument DSC-330). X-ray diffraction patterns were recorded on a Rigaku-denshi diffractometer RINT (Cu Kα: 1.541 A) with an imaging plate.

3.7. Characterization of thin-film structure

Out-of-plane and in-plane X-ray diffraction (XRD) of thin films was acquired using a Rigaku RINT-Ultima X X-ray diffractometer with Cu Kα1 (λ = 1.5418 Å). The surface morphology of thin films was measured in air using a Vecco Dimension 3100 atomic force microscope (AFM). UV-vis absorption spectra were obtained using JASCO V-570 UV–VIS–NIR spectro-photometer. The optical texture of thin films and bulk compounds was observed using an Olympus BX 60 polarized optical microscope.

3.8. Time-of-flight measurement

The time-of-flight setup comprised an Nd:YAG pulse laser equipped with a THG non-linear optical crystal (Continuum Minilite I FN, wavelength = 356 nm, pulse width = 2 ns), hand-made hot stage, source measurement unit (Advantest R-8252) as a DC voltage source, and digital oscilloscope (Tektornics TDS3044B). The liquid crystal compounds were capillary-filled into cells consisting of two ITO-coated glass plates on a hot stage heated above the mesophase–isotropic phase transition temperature. The liquid crystal cell was mounted on the hot stage. Under the application of the electric field by the DC voltage source, the pulse laser light was illuminated on the liquid crystal cell. The induced transient photocurrent was recorded in the digital oscilloscope through a serial resistor (100 Ω).

3.9. Fabrication and characterization of field-effect transistors

Thin films of compound **2** were prepared by the spin-coating method. Then, 0.5–0.7% chlorobenzene solution was spun on doped Si wafers with a 300-nm SiO_2 layer. Thin films of compound **5** were grown by solution casting of 0.1–0.2% solution in chlorobenzene at 70 °C. The preparation by spin-coating was not successful because the films prepared were too thin (<10 nm) and uncontinuous even at a low rotation speed of the spin coater. Prior to film deposition, the wafer was cleaned in a UV ozone cleaner and subsequently treated with hexamethyldisilazane (HMDS). After film deposition, samples of **2** and **5** were annealed in a vacuum oven at 85–90 °C and 110 °C for 10 min, respectively. Gold source and drain electrodes with a thickness of 60 nm were deposited under high vacuum (10^{-4} Pa) through a shadow mask to define the top-contact FET structure with a channel length of 20–30 μm and channel width of 5 mm. Transistor characteristics were measured using a two-channel source meter (Kethley 2612) in a light-shield box under ambient conditions with low humidity or in a vacuum of 10^{-3} Torr. The temperature-dependent electrical measurement of the TFTs was performed over a temperature range of 25 °C to 120 °C on a hot stage, where the temperature was controlled using a PID thermo-controller with an accuracy of 0.1 °C.

Acknowledgments

This work is financially supported by a NEDO Industrial Technology Research Grant, Grant in Aid for Scientific Research (No. 19550183) from the Ministry of Education and Culture, and Research Grant from Asahi Glass Company. We thank the Nano-Processing Facility in National Institute of Advanced Industrial Science and Technology (AIST) for providing the XRD and AFM apparatus and Dr. Hiroyuki Minamikawa for assistance with X-ray diffraction measurement. We also thank Dr. R. Azumi and Dr. M. Chikamatsu of Photonics Research Institute of AIST for fruitful discussions on the characterization of the FET devices, and Prof. T. Kato for his valuable comment on the material design.

References

[1] Z. Bao, A. Dodabalapur, A.J. Lovinger, Appl. Phys. Lett. 69 (1996) 4108.
[2] B.S. Ong, Y. Wu, P. Liu, S. Gardner, J. Am. Chem. Soc. 126 (2004) 3378.
[3] R.J. Kline, M.D. McGehee, M.F. Toney, Nature Mater. 5 (2006) 222.
[4] M.M. Payne, S.R. Parkin, J.E. Anthony, C.-C. Kuo, T.N. Jackson, J. Am. Chem. Soc. 127 (2005) 4986.
[5] A.R. Murphy, P.C. Chang, P. VanDyke, J. Liu, J.M.J. Fréchet, V. Subramanian, D.M. DeLongchamp, S. Sambasivan, D.A. Fischer, E.K. Lin, Chem. Mater. 17 (2005) 6033.
[6] M. Funahashi, Transworld Res. Network, Recent Develop. Appl. Phys. 6 (2003) 839.
[7] Y. Shimizu, K. Oikawa, K. Nakayama, D. Guillon, J. Mater. Chem. 17 (2007) 4223.
[8] S. Sergeyev, W. Pisula, Y.H. Geerts, Chem. Soc. Rev. 36 (2007) 1902.
[9] H. Maeda, M. Funahashi, J. Hanna, Mol. Cryst. Liq. Cryst. Sci. Technol. Sect. A 346 (2000) 183.
[10] A. Pecchia, O.R. Lozman, B. Movaghar, N. Boden, R.J. Bushby, Phys. Rev. B 65 (2002) 104204.
[11] D. Adam, F. Closs, T. Frey, D. Funhoff, D. Haarer, H. Ringsdorf, P. Schuhmacher, K. Siemensmeyer, Phys. Rev. Lett. 70 (1993) 457.
[12] D. Adam, P. Schuhmacher, J. Simmerer, L. Häußling, K. Siemensmeyer, K.-H. Etzbach, H. Ringsdorf, D. Haarer, Nature 371 (1994) 141.
[13] M. Funahashi, J. Hanna, Phys. Rev. Lett. 78 (1997) 2184.
[14] M. Funahashi, J. Hanna, Appl. Phys. Lett. 71 (1997) 602.
[15] M. Funahashi, J. Hanna, Appl. Phys. Lett. 76 (2000) 2574.
[16] M. Funahashi, J. Hanna, Adv. Mater. 17 (2005) 594.
[17] S.R. Farrar, A.E.A. Contoret, M. O'Neill, J.E. Nicholls, G.J. Richards, S.M. Kelly, Phys. Rev. B 66 (2002) 125107.
[18] M. Funahashi, N. Tamaoki, ChemPhysChem. 7 (2006) 1193.
[19] K.L. Woon, M.P. Aldred, P. Vlachos, G.H. Mehl, T. Stirner, S.M. Kelly, M. O'Neill, Chem. Mater. 18 (2006) 2311.
[20] M. Funahashi, N. Tamaoki, Chem. Mater. 19 (2007) 608.
[21] A.J.J.M. van Breemen, P.T. Herwig, C.H.T. Chlon, J. Sweelssen, H.F.M. Schoo, S. Setayesh, W.M. Hardeman, C.A. Martin, D.M. de Leeuw, J.J.P. Valeton, C.W.M. Bastiaansen, D.J. Broer, A.R. Popa-Merticaru, S.C.J. Meskers, J. Am. Chem. Soc. 128 (2006) 2336.
[22] K. Oikawa, H. Monobe, K. Nakayama, T. Kimoto, K. Tsuchiya, B. Heinrich, D. Guillon, Y. Shimizu, M. Yokoyama, Adv. Mater. 19 (2007) 1864.
[23] M. Funahashi, F. Zhang, N. Tamaoki, Adv. Mater. 19 (2007) 353.
[24] F. Zhang, M. Funahashi, N. Tamaoki, Appl. Phys. Lett. 91 (2007) 063515.
[25] A.S. Matharu, S.J. Cowling, G. Wright, Liq. Cryst. 34 (2007) 489.
[26] D. Sainova, S. Janietz, U. Asawapirom, L. Romaner, E. Zojer, N. Koch, A. Vollmer, Chem. Mater. 19 (2007) 1472.
[27] M. Lafrance, C.N. Rowley, T.K. Woo, K. Fagnou, J. Am. Chem. Soc. 128 (2006) 8754.
[28] K. Oikawa, H. Monobe, J. Takahashi, K. Tsuchiya, B. Heinrich, D. Guillon, Y. Shimizu, Chem. Commun. (2005) 5337.
[29] M.-H. Yoon, A. Facchetti, C.E. Stern, T.J. Marks, J. Am. Chem. Soc. 128 (2006) 5792.
[30] Y. Kanemitsu, N. Shimizu, K. Suzuki, Y. Shiraishi, M. Kuroda, Phys. Rev. B 54 (1996) 2198.
[31] A. Facchetti, M.-H. Yoon, C.L. Stern, G.R. Hutchison, M.A. Ratner, T.J. Marks, J. Am. Chem. Soc. 126 (2004) 13480.
[32] D.J. Crouch, P.J. Skabara, J.E. Lohr, J.J.W. McDouall, M. Heeney, I. McCulloch, D. Sparrowe, M. Shkunov, S.J. Coles, P.N. Horton, M.B. Hursthouse, Chem. Mater. 17 (2005) 6567.
[33] R.G. Kepler, Phys. Rev. 119 (1960) 1226.

[34] G. Horowitz, R. Hajlaoui, P. Delannoy, J. Phys. III 5 (1995) 355.
[35] R.J. Chesterfield, J.C. McKeen, C.R. Newman, P.C. Ewbank, D.A. Da Silva Filho, J.-L. Bredas, L.L. Miller, K.R. Mann, C.D. Frisbie, J. Phys. Chem. B 108 (2004) 19281.
[36] R.J. Chesterfield, C.R. Newman, T.M. Pappenfus, P.C. Ewbank, M.H. Haukaas, K.R. Mann, L.L. Miller, C.D. Frisbie, Adv. Mater. 15 (2003) 1278.
[37] S. Mohapatra, B.T. Holmes, C.R. Newman, C.F. Frendergast, C.D. Frisbie, M.D. Ward, Adv. Funct. Mater. 14 (2004) 605.
[38] V. Podzorov, E. Menard, A. Borissov, V. Kiryukhin, J.A. Rogers, M.E. Gershenson, Phys. Rev. Lett. 93 (2004) 086602.
[39] A. Facchetti, M.-H. Yoon, C.L. Stern, H.E. Katz, T.J. Marks, Angew. Chem. Int. Ed. 42 (2003) 3900.
[40] A. Facchetti, M. Mushrush, M.-H. Yoon, G.R. Hutchison, M.A. Ratner, T.J. Marks, J. Am. Chem. Soc. 126 (2004) 13859.
[41] L.-L. Chua, J. Zaumseil, J.-F. Chang, E.C.-W. Ou, P.K.-H. Ho, H. Sirringhaus, R.H. Friend, Nature 434 (2005) 194.
[42] Y. Geng, A. Fechtenkötter, K. Müllen, J. Mater. Chem. 11 (2001) 1634.